Journal of Structural Chemistry. Vol. 56, No. 5, pp. 900-906, 2015.

GAS-PHASE DEPOSITION OF COMPLEX HIGH-MELTING COATINGS ON CARBON FIBER MATERIAL

V. V. Lozanov[1], N. I. Baklanova[1], and N. B. Morozova[2]

UDC 621.793.3

The possibility of modifying carbon materials by RCVD and MOCVD of complex high-melting coatings consisting of the inner hafnium carbide layer and the outer iridium layer is studied. The morphological features, microstructure, and phase composition of the carbide and complex HfC–Ir coating on a carbon material are examined by scanning electron microscopy and powder X-ray diffraction analysis. The HfC coating is uniform, continuous, repeating the geometry of a carbon substrate. A scheme of chemical reactions describing the processes of hafnium transfer on carbon in the form of gaseous hafnium fluorides with a lower valence is proposed. The iridium coating consists of slightly elongated crystallites and has a good adhesion to the carbide layer.

DOI: 10.1134/S002247661505011X

Keywords: vapor deposition, hafnium carbide, iridium, coatings, carbon fiber material.

In recent years, the possibility of using iridium coatings to protect carbon materials in the oxidizing media at high temperatures has been intensively studied [1]. Thus, in [2-4], the morphology, composition, and high-temperature response of coatings based on Ir, Ir/Re and laminated Ir–W coatings on graphite were examined. Iridium is chosen as a protective coating for carbon materials due to its high melting point (2720 K), low solubility in carbon, the absence of interactions with carbon up to the eutectic point (~2570 K), and low permeability with respect to oxygen and carbon [4]. In addition, iridium has good mechanical characteristics; the rates of its recession in oxygen are quite low [5, 6].

There are many techniques for applying iridium coatings on carbon materials. These include magnetron sputtering, laser sintering, slip process. As a rule, these methods are used to apply coatings on a flat substrate [7]. Another group are the electrochemical methods to reduce iridium from solutions or fused salt mixtures, for example, from fused NaCl–KCl–CsCl–$IrCl_3$ [7]. A disadvantage of these methods is that the precursors can penetrate into the substrate, which is highly undesirable.

One of the most efficient methods of forming iridium coatings is metal-organic chemical vapor deposition (MOCVD). The MOCVD process allows the precision control of the thickness and texture of coatings by varying the deposition parameters. The distinctive advantages of the method are its relative instrumental simplicity, the possibility to obtain uniform layers on the products with complex configuration at rather low temperatures, cost effectiveness due to a minimal consumption of the initial precursor, which is especially important with the deposition of iridium layers.

To deposit iridium layers, volatile coordination and metal-organic compounds of iridium are generally used as precursors [8]. One of the problems with the above mentioned techniques is poor adhesion of iridium coating to carbon. In

[1]Institute of Solid State Chemistry and Mechanochemistry, Siberian Branch, Russian Academy of Sciences, Novosibirsk, Russia; baklanova@solid.nsc.ru. [2]Nikolaev Institute of Inorganic Chemistry, Siberian Branch, Russian Academy of Sciences, Novosibirsk, Russia. Translated from *Zhurnal Strukturnoi Khimii*, Vol. 56, No. 5, pp. 958-965, September-October, 2015. Original article submitted April 9, 2015.

order to solve this problem, an approach involving the application of an intermediate carbide layer, for example, from titanium carbide or hafnium carbide [9], on carbon substrate using EB-PVD and CVD was previously proposed.

We chose the RCVD (reactive chemical vapor deposition) and MOCVD methods for applying complex hafnium carbide–iridium coatings on carbon materials.

Therefore, the work is aimed to examine the possibility of modifying carbon materials by deposition of complex high-melting coatings consisting of the inner layer of high-melting hafnium carbide and the outer iridium layer using RCVD and MOCVD.

EXPERIMENTAL

Precursors. The metal cuttings prepared from hafnium iodide GFI-1 (GOST 22517-77, content of Hf+Zr > 99.8% (wt)) was used to form the coatings of hafnium carbide. Freon-14 (R14, TU 301-***14***-78-92, volume fraction of CF_4 no less than 99.3%) was used as a reagent gas.

Tris-acetylacetonate of iridium(III) (hereafter, $Ir(acac)_3$) was used to deposit the iridium coatings. The synthesis of $Ir(acac)_3$ was performed using our proprietary technique [10] from hexafluoro complexes of iridium. The compound was purified by zone sublimation at $P = 10^{-2}$ Torr and $T = 150$°C. The yield (yellow crystals) was 90% ($T_{melt.}$ 269-270°C). The individuality of the isolated phase $Ir(acac)_3$ is confirmed by the data of elemental and powder X-ray diffraction analysis, using IR spectroscopy and mass spectroscopy.

The temperature dependence of the saturated vapor pressure over $Ir(acac)_3$ was measured by the Knudsen effusion method with mass spectroscopic measurement of the gas-phase composition. We obtained the following thermodynamic parameters (measurement range 110-160°C): $\ln(P, \text{at}) = 27.0 - 15701/(T, \text{K})$; ΔH_{T*} (kJ/mol) = 130.5±3.4; ΔS^0_{T*} (J/mol·K) = = 224.4±8.2 [11].

Carbon fiber materials of the “Ural” grade (the main component content of no less than 99%, GOST 28005-88) were used as the substrates for coating application.

Application of coatings. The experiments for deposition of hafnium carbide on a carbon material substrate were carried out at the temperature of 1000°C in a quartz reactor. Before the reagent gas was introduced, the system was thoroughly degased at 1000°C and then cooled. The reagent gas was introduced into a cool vessel, then the vessel was sealed and set into a furnace, which was subsequently heated in a predetermined mode; the vessel was kept at a given temperature and spontaneously cooled.

The processes of $Ir(acac)_3$ vapor deposition of iridium coatings were carried out in a device (vertical cold-wall reactor) at atmospheric pressure [12]. We used hydrogen as a reagent gas (2 l/h) and argon as a carrier gas (1 l/h). The complex hafnium carbide–iridium coatings on the carbon materials were obtained at the deposition temperature of 550°C, evaporator temperature of 210°C; the experiment time was 4 h.

Characterization of samples. The microstructure of the initial and modified carbon materials was studied by means of high resolution scanning electron microscopy (SEM) on the MIRA3 TESCAN and TM-1000 microscopes (Hitachi Ltd., Japan). The samples were predeposited with a nanosized layer of chromium (MIRA3 TESCAN). The elemental composition of the coatings was studied using energy dispersive microanalysis on a SwiftED-TM module (Hitachi Ltd., Japan).

The powder X-ray diffraction (XRD) analysis was performed on a D8 Advance diffractometer (Bruker, Germany) with the characteristic $K\alpha$ radiation from a copper anode ($\lambda_1 = 1.54056$ Å, $\lambda_2 = 1.54439$ Å). The obtained diffraction patterns were analyzed with the DIFFRAC^{plus} software using the ICDD PDF-2 database (2008). The unit cell parameters and the sizes of coherent scattering regions (CSR) were refined with the TOPAS 4.2 software for profile and structural analysis using the ICSD crystal structure database (1997). The carbon-to-metal ratio in carbides was determined according to Vegard’s law [13, 14]. Based on the literature data [15], we constructed the dependence of the HfC_x lattice parameter a on its composition and approximated it by the straight line $y = A + Bx$ according to the least squares technique. Using the TOPAS 4.2 software, from the experimental diffraction patterns we determined the carbide lattice parameter. From the equations $y = A + Bx$, the x

values for HfC_x were calculated. We estimated the maximum absolute error of determination of the obtained relationships [16]. For x, the upper limit of possible absolute error of determination is found as follows:

$$\delta x = \frac{\delta y}{B} + \frac{\delta A}{B} + \frac{(y - A)\delta B}{B^2}.$$

The δA and δB parameters are the absolute errors of the A and B values obtained in the construction of the approximation straight line in the Origin 6.1 software; δy is the error of determination of y (the crystal lattice parameter).

The morphology of the crystals of monoclinic HfO_2 was modeled using the JCRYSTAL software. For the modeling, the data on m-HfO_2 # 34-104 (the ICDD PDF-2 database (2008)) were used.

RESULTS AND DISCUSSION

Formation of HfC coatings on carbon materials. After the RCVD process, the sample of carbon material acquires grey metallic lustre typical of hafnium carbide. The powder XRD results confirm that under RCVD in the Hf–C–F system at different exposure times (24 h and 48 h) the hafnium carbide coatings form on the carbon substrate (Fig. 1). Besides the intensive peaks corresponding to hafnium carbide, the X-ray diffraction pattern has the reflections belonging to the disordered graphite-like carbon, with the peaks at $2\theta \sim 25.5°$, 43°, 53°, 78.5°.

With the full-profile powder XRD analysis, we obtained the values of the unit cell parameter. Determination of the carbon content in the HfC_x compound by the equation $y(a) = A + Bx$ has some distinctive features, that is: for HfC_x in a range $x = 0.62$-1.00, there is a positive deviation from the Vegard law at $x = 0.83$, which, as it was noted in [14, 15, 17, 18], can be due to the presence of ordered Hf_6C_5 and Hf_3C_2 superstructures. Based on the data from [15], according to the dependence of the lattice parameter a on the composition x for the HfC_x phase, we constructed the approximation straight lines for the ranges $x = 0.83(0)$-1.00 and $x = 0.62$-0.83 respectively using the least square method. The graphs of a dependence on x are shown in Fig. 2*a*, *b*. Then, from the values of the parameter a calculated from the X-ray diffraction patterns of the products obtained under different conditions, the stoichiometry of the products was determined. Thus, for the exposure time of 24 h, x was 0.95-0.97, and for 48 h exposure x was 0.90-0.93. From the obtained data it follows that with an increase in the exposure time, the composition of the coating shifts to the lower boundary of the homogeneity region.

Fig. 3 shows the electron-microscopic images of the HfC coating on the carbon substrate (exposure time of 24 h). The coating repeats complex geometry of the carbon substrate, with pores and, in some places, discontinuity of the coating. Flat regions of the coating consist of grains of several tens of nanometers in size.

The analysis of cuttings used as a hafnium source showed that it became fragile and dark grey. According to the powder XRD data, the product formed in place of hafnium metal is a mixture of the hafnium carbide and silicide phases, with

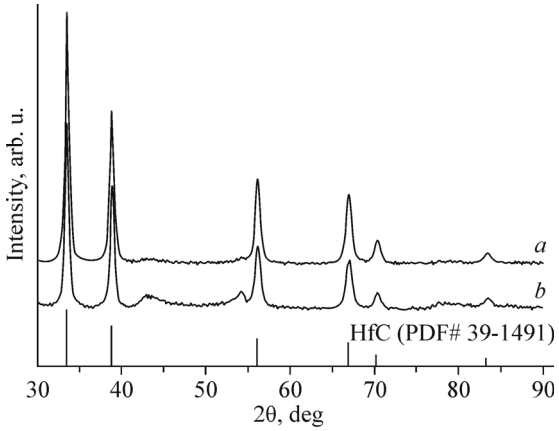

Fig. 1. Diffraction patterns of the carbon sample with coatings obtained using RCVD in the Hf–C–F system depending on the duration of the experiment: 24 h (*a*); 48 h (*b*).

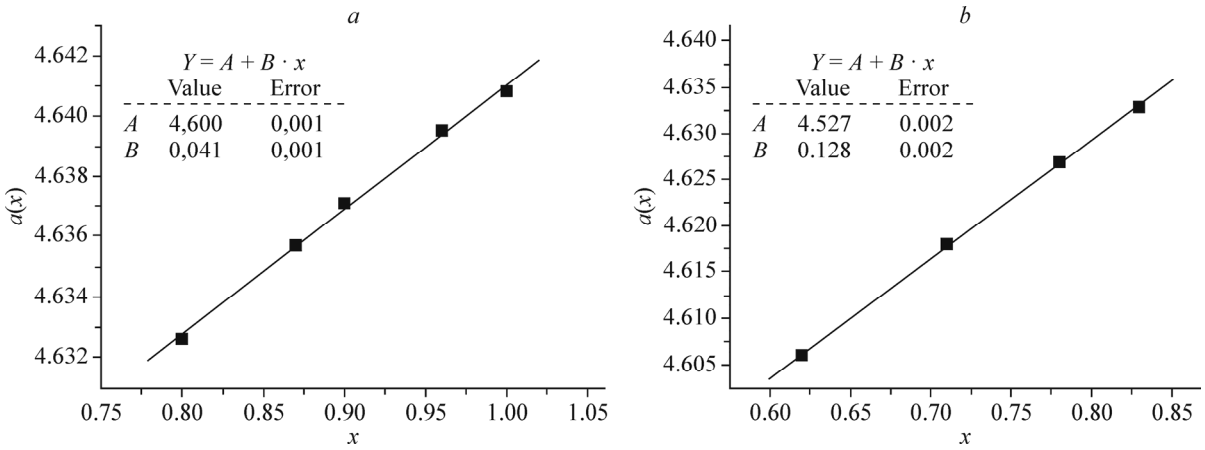

Fig. 2. Graphs of the dependences of the lattice parameter a on x for the HfC_x phase: with high carbon content (0.80-1.00) (*a*); with low carbon content (0.62-0.83) (*b*).

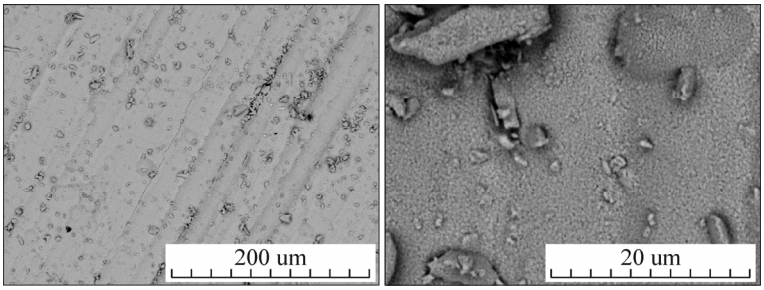

Fig. 3. Electron microscopic images of the surface of the carbon sample with the HfC coating (exposure time 24 h).

a predominance of the latter (Fig. 4). Note that the peaks of hafnium metal do not appear at all, which can evidence its complete transformation into the above mentioned compounds.

On the walls of the quartz reactor, we found a large amount of condensate, which, according to the powder XRD data, is a phase of monoclinic hafnium dioxide (Fig. 5). Since the only source of oxygen are the walls of the quartz reactor, it can be expected that SiO_2 reacts with the gas phase components, for example, hafnium and carbon fluorides, with the formation of volatile oxygen-containing compounds of hafnium and silicon [19-21], which interaction, in turn, results in deposition of hafnium dioxide.

Previously, we proposed a scheme of formation of hafnium carbide on carbon under conditions of chemical transport through the gas phase [19]. According to this scheme, the formation of hafnium carbide on metal cuttings can be due to the reaction

$$2Hf_{(s)} + CF_{4(g)} = HfC_{(s)} + HfF_{4(g)}. \quad (1)$$

Although there are almost no data in the literature on gaseous lower-valence hafnium fluorides, the transfer of hafnium through the gas phase in the Hf–C–F system (where C is the carbon fiber) discovered by us earlier [19] allows us to expect their existence in the gas phase. Gaseous hafnium tetrafluoride can react with hafnium metal forming lower valence fluorides of hafnium (reaction (2)), which, in turn, react with carbon forming hafnium carbide (reaction (3)):

$$(4 - n)Hf_{(s)} + nHfF_{4(g)} = 4HfF_{n(g)}, \quad \text{where } n = 3, 2, 1, \quad (2)$$

$$(4 - n)C_{(s)} + 4HfF_{n(g)} = nHfF_{4(g)} + (4 - n)HfC_{(s)}. \quad (3)$$

Note that, in the process of depositing hafnium carbide on carbon substrate using RCVD in a flow, rather than a closed quartz reactor, on the cold parts of the reactor the condensate was found, which composition corresponds to monoclinic hafnium tetrafluoride. Its formation can be described by reaction (1). A somewhat different picture is observed when the process is carried out in a closed reactor, the entire volume of which is in a hot zone. In this case, hafnium tetrafluoride does not remove from the reaction zone by condensation on the cold parts of the reactor, but remains in the hot

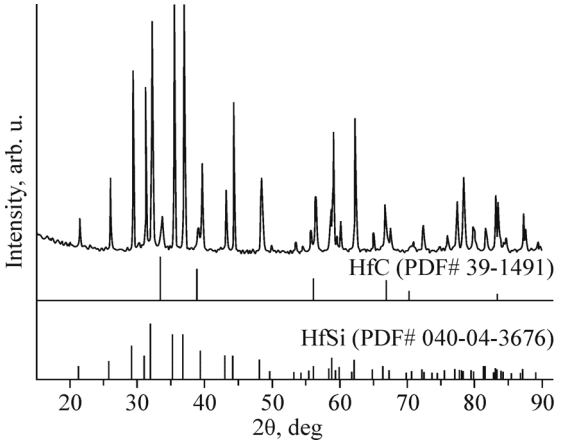

Fig. 4. X-ray diffraction pattern of the products formed on the hafnium cuttings during the RCVD process.

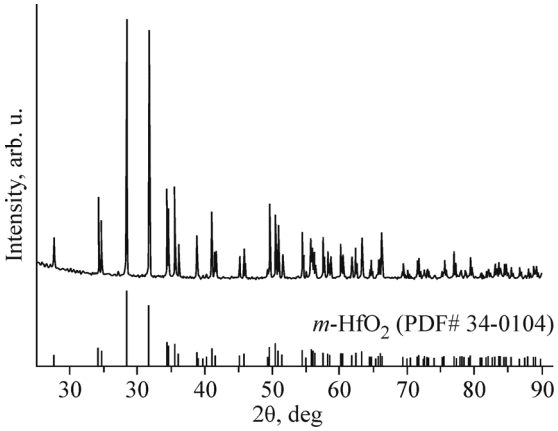

Fig. 5. X-ray diffraction pattern of the condensate formed on the walls of a quartz reactor during the RCVD process in the Hf–C–F system.

zone of the reactor and reacts with its quartz walls. Accumulation of a large amount of HfO_2 crystals evidences that, alongside with the solid/gas reaction (4), there can also occur the reactions of gaseous oxygen-containing reagents resulting in deposition of solid monoclinic hafnium dioxide, for example, reactions (6), (8), and (10). It should be noted that an issue on the chemistry of the processes occurring in the Hf–C–F–Si–O system requires a special consideration and is the subject of future research.

$$SiO_{2(s)} + HfF_{4(g)} = SiF_{4(g)} + HfO_{2(s)}, \quad (4)$$

$$HfF_{4(g)} + SiO_{2(s)} = HfOF_{2(g)} + SiOF_{2(g)}, \quad (5)$$

$$2HfOF_{2(g)} = HfO_{2(s)} + HfF_{4(g)}, \quad (6)$$

$$HfF_{4(g)} + SiOF_{2(g)} = HfOF_{2(g)} + SiF_{4(g)}, \quad (7)$$

$$2SiOF_{2(g)} + HfF_{4(g)} = HfO_{2(s)} + 2SiF_{4(g)}, \quad (8)$$

$$SiO_{2(s)} + SiF_{4(g)} = 2SiOF_{2(g)}, \quad (9)$$

$$HfOF_{2(g)} + SiOF_{2(g)} = HfO_{2(s)} + SiF_{4(g)}. \quad (10)$$

As pointed above, we found not only hafnium carbide (reaction (3)), but also hafnium silicide HfSi on hafnium metal. Its formation is likely due to reaction (11):

$$2Hf_{(s)} + SiF_{4(g)} \rightarrow HfSi_{(s)} + HfF_{4(g)}. \quad (11)$$

Study of the crystals of monoclinic hafnium dioxide, which grow directly on the reactor surface, indicates that they take the form of octahedral pyramids of up to 15 μm from base to vertex. The modeling of the crystal morphology shows that the formation of such structures is probably occurs with the involvement of the planes with the indices *hkl* (–112) and (–121) having the interplanar distances $d = 2.2010$ Å and 2.1678 Å respectively (Fig. 6*a*, *b*). On the pyramidal crystals, the transparent platy crystals of monoclinic HfO_2 grew, which reached macroscopic size (Fig. 6*c*). Both on the pyramidal and platy crystals, there are evident growth stages (Fig. 6*d*).

Estimation of the thickness of hafnium carbide coating formed on the carbon substrate in the result of interaction between gaseous hafnium subfluorides and carbon, shows that the thickness insignificantly increases with time. It is possible that the reaction for obtaining hafnium carbide slows down due to a hindered access of gaseous hafnium subfluorides to carbon substrate through a layer of relatively dense coating formed (Fig. 4). This is also supported by the data of powder X-ray diffraction analysis. Indeed, for the exposure time of 24 h the composition of the HfC_x coating is shifted to the lower boundary of the homogeneity region. At large exposure times, the composition of the coatings gradually approximates to stoichiometric one.

Complex hafnium carbide–iridium coating on carbon material. The samples of complex HfC–Ir coating on a carbon material after application of iridium layer acquire a metallic lustre. The powder XRD analysis of the samples shows the peaks corresponding only to hafnium carbide and iridium metal (Fig. 7). The iridium coating on the samples is rather thick and causes the shielding of the carbide layer, which peaks are weakly manifested.

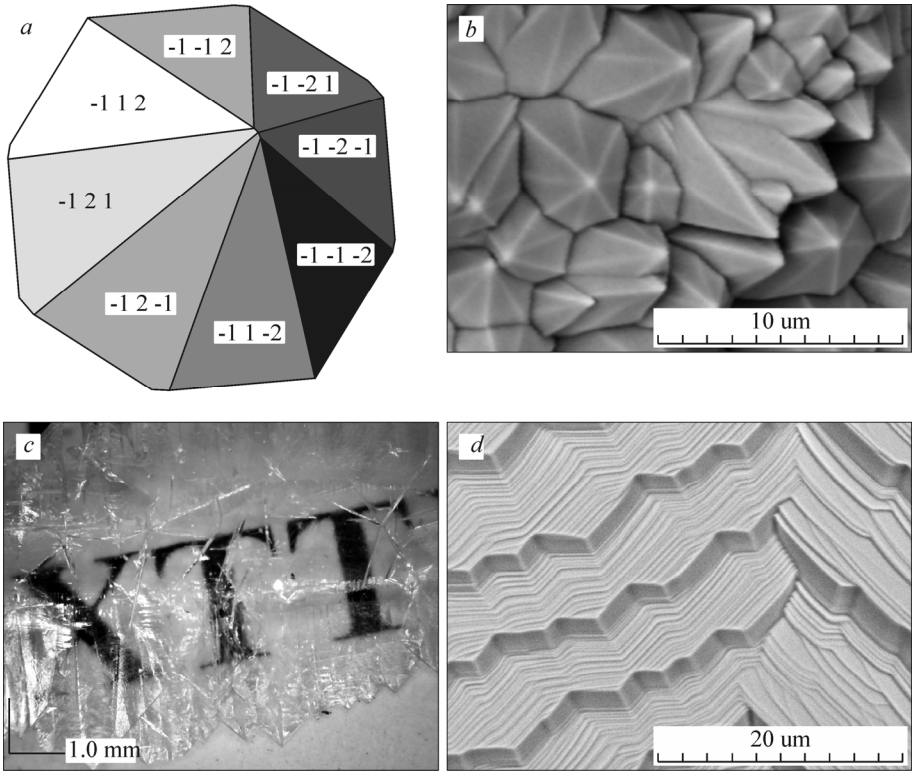

Fig. 6. Electron-microscopic images of the condensed *m*-HfO_2: model of the *m*-HfO_2 crystal habit (*a*); pyramidal crystals grown on the reactor surface (*b*); growth stages on the pyramid planes (*c*); growth stages on the transparent plates (*d*).

The coating structure is well seen in Fig. 8. The inner carbide layer is very dense and consists of nanosized crystallites, while the outer iridium layer consists of larger slightly elongated grains. As is evident from the electron-microscopic images, the iridium coating has a columnar structure, with almost no cracks, pores, and flaking. The iridium layer is rather dense and weakly textured (Fig. 8). The HfC and Ir layers are in good cohesion with each other; there is a clear boundary between them. According to the SEM data, the overall thickness of the complex HfC–Ir coating is 1.2-1.5 μm. Application of the iridium layer causes a partial flaking of multilayer HfC–Ir coating.

In conclusion, we carried out the experiments for obtaining the carbide and complex HfC–Ir coatings on carbon materials using RCVD and MOCVD. The HfC coating is uniform, repeating a complex geometry of carbon substrate, the grains are several tens nanometers in size. According to the powder XRD data, when the HfC coatings are deposited in a closed system, the phase of monoclinic HfO_2 is found on the reactor walls and those of hafnium silicide HfSi and HfC are

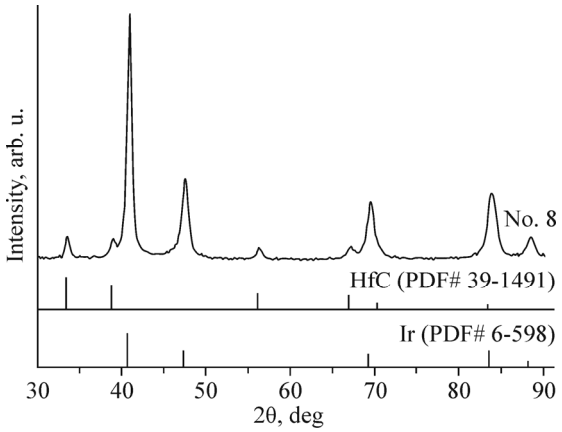

Fig. 7. Diffraction pattern of the complex HfC–Ir coating on carbon.

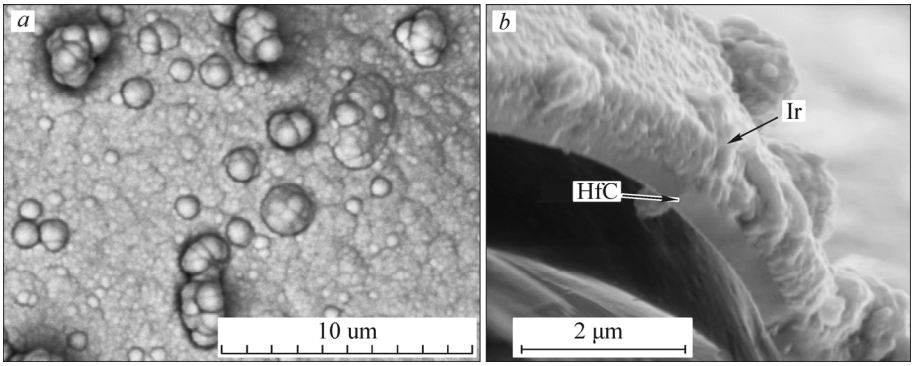

Fig. 8. Electron-microscopic images of the complex HfC–Ir coating on carbon: general view (*a*); cross-section of the coating (*b*).

detected on the initial Hf metal. An overall thickness of the complex HfC–Ir coating is 1-1.5 μm. There is a clear boundary between the inner carbide layer and the outer iridium layer, which have a good mechanical adhesion with each other. Application of iridium layer causes partial flaking of the complex coating.

The authors are grateful to Dr. N. V. Bulina (Institute of Solid State Chemistry and Mechanochemistry, Siberian Branch of RAS) for measurement of X-ray diffraction patterns.

The work was performed with the support of the grant of the RF President for support leading scientific schools NSh-2938.2014.3, contract No. 779-7-2013, and with the support of the grant of the Ministry of Education and Science of the RF (contract No. 14.604.21.0080 from June 30, 2014, unique identifier for applied research RFMEFI60414X0080).

REFERENCES

1. Z. Chen, W. Wu, H. Cheng, et al., *Acta Astronaut*., **66**, Nos. 5/6, 682 (2010).
2. W. Wu, Z. Chen, H. Cheng, et al., *Appl. Surf. Sci*., **257,** 7295 (2011).
3. S. Bai, L. Zhu, H. Zhang, et al., *Int. J. Refract. Met. Hard Mater*., **41,** 563 (2013).
4. W. Wu and Z. Chen, *J. Wuhan Univ. Technol., Mater. Sci. Ed*., **27**, No. 4, 652 (2012).
5. N. I. Baklanova, V. V. Lozanov, N. B. Morozova, et al., *Thin Solid Films*, **578,** 148 (2015).
6. R. T. Wimber, S. W. Hills, N. K. Wahl, et al., *Metall. Trans. A*, **8A,** 193 (1977).
7. E. K. Ohriner, *Platinum Met. Rev*., **52**, No. 3, 186 (2008).
8. V. Yu. Vasilyev, N. B. Morozova, T. V. Basova, et al., *RSC Adv*. (2015); doi: 10.1039/c5ra03566j.
9. J. R. Strife, J. G. Smeggil, and W. L. Worrel, *J. Am. Ceram. Soc*., **73**, No. 4, 838 (1990).
10. I. K. Igumenov, V. G. Isakova, N. B. Morozova, et al., *Patent EA N000402*, 09.04.99.
11. N. B. Morozova, P. P. Semyannikov, S. V. Sysoev, et al., *J. Therm. Anal. Calorim*., **60,** 489 (2000).
12. I. K. Igumenov, N. V. Gelfond, N. B. Morozova, et al., *Chem. Vap. Deposition*, **13,** 633 (2007).
13. A. R. Denton and N. W. Ashcroft, *Phys. Rev. A*, **43,** 3161 (1991).
14. A. West, *Solid State Chemistry and Its Applications*, John Wiley & Sons (1987).
15. A. I. Gusev and A. N. Zyryanova, *Phys. Status Solidi A*, **177,** 419 (2000).
16. I. V. Mironov, *Introduction to Optical Methods of Analysis: Tutorial* [in Russian], NGU, Novosibirsk (2006).
17. A. I. Gusev and A. N. Zyryanova, *JETP Lett*., **69**, No. 4, 324 (1999).
18. V. I. Zhelankin and B. S. Kutsev, *J. Struct. Chem*., **4**, No. 6, 796-798 (1963).
19. N. I. Baklanova, T. M. Zima, A. I. Boronin, et al., *Surf. Coat. Technol*., **201**, No. 6, 2313 (2006).
20. H. Vogt, A. Fischer, G. Grosser, et al., *Z. Anorg. Allg. Chem*., **551**, No. 8, 223 (1987).
21. R. W. Baier and R. C. Oliver, *Chemical Corrosion of Rocket Liner Materials and Propellant Performance Studies. Thermodynamic Properties of Heavy Metal Species: Final technical report, N NOw-61-0905-c*, vol. 2, Washington, D. C. (1963), p. 99.